THE JOURNAL OF BIOLOGICAL CHEMISTRY
Vol. 276, No. 35, Issue of August 31, pp. 33027–33035, 2001

Printed in U.S.A.

Mechanisms of pH Regulation in the Regulated Secretory Pathway*

Received for publication, May 1, 2001, and in revised form, June 11, 2001
Published, JBC Papers in Press, June 11, 2001, DOI 10.1074/jbc.M103917200

Minnie M. Wu‡§, Michael Grabe¶‖, Stephen Adams, Roger Y. Tsien**, Hsiao-Ping H. Moore‡, and Terry E. Machen‡ ‡‡**

*From the ‡Department of Molecular and Cell Biology, University of California, Berkeley, California 94720-3200, the ¶Department of Physics, University of California, Berkeley, California 94720-3112, and the **Department of Pharmacology and Howard Hughes Medical Institute, University of California, San Diego, La Jolla, California 92093-0647*

A precise pH gradient between organelles of the regulated secretory pathway is required for sorting and processing of prohormones. We studied pH regulation in live endocrine cells by targeting biotin-based pH indicators to cellular organelles expressing avidin-chimera proteins. In AtT-20 cells, we found that steady-state pH decreased from the endoplasmic reticulum (ER) (pH_{ER} = 7.4 ± 0.2, mean ± S.D.) to Golgi (pH_G = 6.2 ± 0.4) to mature secretory granules (MSGs) (pH_{MSG} = 5.5 ± 0.4). Golgi and MSGs required active H^+ v-ATPases for acidification. ER, Golgi, and MSG steady-state pH values were also dependent upon the different H^+ leak rates across each membrane. However, neither steady-state pH_{MSG} nor rates of passive H^+ leak were affected by Cl^--free solutions or valinomycin, indicating that MSG membrane potential was small and not a determinant of pH_{MSG}. Therefore, our data do not support earlier suggestions that organelle acidification is primarily regulated by Cl^- conductances. Measurements of H^+ leak rates, buffer capacities, and estimates of surface areas and volumes of these organelles were applied to a mathematical model to determine the H^+ permeability (P_{H+}) of each organelle membrane. We found that P_{H+} decreased progressively from ER to Golgi to MSGs, and proper acidification of Golgi and MSGs required gradual decreases in P_{H+} and successive increases in the active H^+ pump density.

Maintenance of lumenal pH in organelles of the secretory pathway is required for proper sorting and proteolytic processing of prohormones. Even small pH differences between organelles can be critical in separating cellular events. For example, a difference of <0.5 pH can determine whether a prohormone is processed (1). In professional secretory cells (*e.g.* endocrine and neuroendocrine), "regulated" secretory proteins have been hypothesized to be sorted from constitutively secreted proteins by a process of pH- and calcium-dependent selective aggregation (2–4). The exact site where aggregation occurs is controversial, largely due to the lack of direct measurements of organelle pH along the regulated secretory pathway. The "sorting for entry" model postulates that sorting occurs when proteins encounter the ionic milieu of the trans-Golgi network (3). In contrast, the "sorting by retention" model asserts that aggregation serves to retain regulated proteins in granules and does not occur until prohormones have entered acidic immature secretory granules (ISGs)[1] and become proteolytically processed (5).

Work by several groups (1, 6–11) using a variety of techniques indicates that organelles of the secretory pathway, from ER to Golgi to secretory granules, become increasingly acidic. Indirect measurements of pH in isolated secretory granules of endocrine and neuroendocrine cells using either electron microscopy (measuring acidity based on accumulation of the weak base DAMP) or biochemical reactions (measuring acidity based on the extent of processing) (1, 6–11) suggested that ISGs and MSGs were both acidic (pH_{ISG} ~6.3–5.7; pH_{MSG} ~5.5–5.0). In live cell pH measurements using the green fluorescent protein derivative pHlorin (12), secretory granules of mast cells were also acidic (pH 5.2). In "non-regulated" cells (Chinese hamster ovary, HeLa, HepG2, and Vero), pH experiments performed using both DAMP on fixed cells (13, 14) and fluorescent probes in live, intact cells (15–21) showed that ER pH (pH_{ER} = 7.1–7.2) was similar to cytosolic pH (pH_c), whereas Golgi pH was acidic (pH_G = 6.5–6.2). In contrast, in "regulated" cells, experiments using DAMP detected no acidification of Golgi in pancreatic islet cells (7, 8). It is unclear whether the conflicting Golgi pH data are due to differences in cell type or techniques used. Therefore, although there is general agreement regarding the acidity of MSGs, the exact pH of Golgi *versus* ISGs (and hence the site of sorting) in regulated secretory cells remains in question.

Furthermore, although the dynamics of pH regulation in the Golgi and ER of non-regulated cells has been extensively studied, there has been no examination of the pH regulatory mechanisms of Golgi and MSGs in live, intact cells with regulated secretory pathways. pH studies of these organelles have been limited to either fixed cells or isolated organelles *in vitro*. Data from these studies suggested that Golgi and secretory granules controlled their acidic pH values by altering their conductances to Cl^-, which served as a counterion for the H^+ v-ATPase (6, 9). Experiments on isolated synaptic vesicles also supported a

* This work was supported in part by National Institutes of Health Grants DK51799 (to T. E. M.) and R24RR14891 (to H.-P. H. M.) and National Science Foundation Grant MCB-9983342 (to H.-P. H. M. and T. E. M.). The costs of publication of this article were defrayed in part by the payment of page charges. This article must therefore be hereby marked "*advertisement*" in accordance with 18 U.S.C. Section 1734 solely to indicate this fact.

§ Supported by National Institutes of Health training grants.

‖ Supported by National Science Foundation Grant DMS9220719.

‡‡ To whom correspondence should be addressed: 231 Life Sciences Addition, University of California, Berkeley, CA 94720-3200. Tel.: 510-642-2983; Fax: 510-643-6791; E-mail: machen@socrates.berkeley.edu.

[1] The abbreviations used are: ISGs, immature secretory granules; ER, endoplasmic reticulum; MSGs, mature secretory granules; v-ATPase, vacuolar ATPase; FCCP, carbonyl cyanide *p*-trifluoromethoxyphenylhydrazone; BCECF-AM, 2′,7′-bis-(2carboxyethyl-5-(and-6)-carboxyfluorescein, acetoxymethylester; AV-POMC. avidin-propiomelanocortin; DMEM, Dulbecco's modified Eagle's medium; ODE, ordinary differential equations; DAMP, 3-(2,4-dinitroanilino)-3′ amino-*N*-methyl dipropylamine.

critical role for Cl^- in organelle acidification (22, 23). These results led to the general hypothesis that acidic organelles maintain distinct lumenal pH values by maintaining different permeabilities to Cl^-, the primary counterion (24). However, experiments in non-regulated cells demonstrated that although Cl^- and K^+ did serve as counterions for H^+ pumping, Cl^- and K^+ conductances were large compared with the passive H^+ conductance, arguing against modulation of Cl^- and K^+ conductances as a mechanism for trans-Golgi network or Golgi pH regulation (18, 21). In addition, the pH-dependent processing of secretogranin II measured *in vitro* was not stimulated by increasing the outside Cl^- concentration (11). Thus, the exact mechanisms regulating acidification along the regulated secretory pathway are unknown.

To begin to address the controversies and the gaps in our understanding of pH regulation in organelles of the regulated secretory pathway, we targeted pH indicators to the ER, Golgi, and MSGs to study the pH regulatory mechanisms in live, intact endocrine cells. We chose the AtT-20 mouse pituitary cell line because it has a well characterized regulated secretory pathway. The data presented in this paper represent the first study of pH regulation in MSGs of live, intact cells, and the first systematic comparison of the pH regulatory mechanisms between the major organelles of the regulated secretory pathway. We tested for the importance of Cl^- and K^+ conductances in determining pH_G and pH_{MSG} by eliminating Cl^- from the solutions and by using the K^+ ionophore valinomycin. In addition, since H^+ leaks appear to be crucial determinants of organelle pH (18, 21, 25), we measured H^+ leak rates and buffer capacities of the ER, Golgi, and MSGs and applied the results to a mathematical model (26) to calculate H^+ permeabilities for each organelle. From our experimental data and mathematical modeling, we found that the acidification step between the ER and Golgi in AtT-20 cells was similar to that in non-regulated cells (21, 25) in that it required both an increase in active H^+ pump density and a reduction of H^+ permeability from the ER to the Golgi. Meanwhile, the acidification step between Golgi and MSGs required a decrease in H^+ permeability in Golgi *versus* MSG membranes.

EXPERIMENTAL PROCEDURES

Materials—Salts, amiloride, FCCP, fluorescein isothiocyanate-dextran, monensin, sodium butyrate, nigericin, puromycin, and valinomycin were from Sigma; all other organic chemicals were from Aldrich; solvents were from Fisher; and restriction enzymes were from New England Biolabs (Beverly, MA). Bafilomycin was from Calbiochem; mouse laminin was from Life Technologies, Inc.; BCECF-AM and Pluronic F-127 were from Molecular Probes, Inc. (Eugene, OR).

Construction of ER, Golgi, and MSG-targeted Avidin-Chimera Proteins—The avidin-KDEL (AV-KDEL)-encoding plasmid was constructed as described (21). An avidin-pro-opiomelanocortin (AV-POMC)-encoding plasmid was constructed by polymerase chain reaction amplification of avidin (Dr. Markku Kulomaa, University of Jyvaskyla, Finland) using primers (5′-cgcgggaagcttgccaccatggtgcacgcaacctcc-3′ and 5′-cgcgggggatcctccttctgtgtgcgcag-3′), which allowed isolation of avidin by *Hin*dIII and *Bam*HI digestion. A signal sequence-lacking POMC was polymerase chain reaction-amplified from mouse POMC (gift from Dr. Edward Herbert) using primers 5′-cgcggggatccctggtgcctggagagcagc-3′ and 5′-cgcgggggcggccgctcactggcccttcttgtg-3′ and isolated by digestion with *Bam*HI and *Not*I. Avidin and POMC were ligated into sIg-7-poly vector (Dr. Brian Seed, Massachusetts General Hospital) using *Hin*dIII, *Bam*HI, and *Not*I sites (avidin replaced Ig).

Cell Culture and Transfection of AtT-20 Cells—AtT-20 cells were grown as described previously (1). Golgi and MSG pH experiments were performed on AtT-20 cells that were either transiently transfected (by electroporation, see below) or stably transfected (27) with AV-POMC DNA. ER pH experiments were performed on AtT-20 cells transiently transfected with AV-KDEL DNA by electroporation.

24 h before electroporation, AtT-20 cells were passaged to obtain a 50% confluent 15-cm dish. On the day of electroporation, cells were trypsinized, rinsed with normal growth medium, and pelleted. The cell pellet was rinsed with cold DMEM, re-pelleted, and resuspended in 300 μl of cold DMEM. 100 μg of AV-POMC or AV-KDEL DNA and 50 μg of a puromycin resistance gene-encoding plasmid (pSFPACEBv, Dr. Brian Seed) were combined, phenol/chloroform-extracted, ethanol-precipitated, and resuspended in 100 μl of DMEM. To electroporate, the 300 μl of cells were mixed with the 100 μl of DNA, incubated for 5 min on ice, and transferred to a cold 0.4-cm gap cuvette. Cells were electroporated at 250 V, 0 ohm resistance, and 960 microfarads using a Bio-Rad Gene Pulser. After electroporation, cells recovered for 10 min on ice before being replated onto a 15-cm plate. 24 h post-transfection, 0.75 μg/ml of puromycin (Sigma) was added to the cell medium to select for positive transfectants. After 48 h of puromycin treatment, cells were replated onto laminin-coated coverslips and allowed to recover 24 h before imaging experiments were performed.

Butyrate Induction of AV-POMC Expression—Because the expression level of AV-POMC in AtT-20 stable cell lines was too low for fluorescence imaging experiments, we used a butyrate incubation protocol, described previously (28), to boost expression of AV-POMC. Butyrate prevents histone deacetylation, inducing expression from viral promoters. AV-POMC stably expressing AtT-20 cells were plated on laminin-coated coverslips; 24 h after plating, cells were incubated in 6 mM sodium butyrate in normal growth medium for 15 h. After butyrate induction, cells were rinsed once in a large volume of DMEM and chased in normal growth medium for at least 34 h before loading with Flubi dyes. The butyrate incubation had no effect on endogenous POMC or AV-POMC processing, indicating that MSG pH was unaffected by this protocol (data not shown).

Fluorescent Labeling of Cytosol, ER, Golgi, and MSGs—Cell cytosol was labeled using BCECF-AM and fluorescein isothiocyanate-dextran as described previously (21, 29).

We used AV-KDEL-expressing AtT-20 cells to monitor ER pH and AV-POMC-expressing AtT-20 cells to monitor the pH of both Golgi and MSGs. To label the avidin-containing lumens of ER, Golgi, and MSGs, the cell-permeable Flubi-2 diacetate (Flubida-2, ~2 mM) was mixed 1:1 with Pluronic F-127 (20% w/v in dry Me_2SO) and then diluted to the desired final concentration with DMEM containing <2% fetal calf serum. AV-KDEL- or AV-POMC-expressing cells were rinsed with DMEM, loaded with 2–4 μM Flubida-2 dye for 4–6 h, and then chased with normal growth medium for 0–2 h (0 h of chase for Golgi measurements; >2 h of chase for MSG measurements) at 37 °C.

Fluorescence Ratio Imaging of Cytosolic, ER, Golgi, and MSG pH—Cytosol, ER, Golgi, and MSG pH values were measured in separate experiments using digitally processed fluorescence ratio imaging. Ratio imaging measurements were performed at room temperature as described previously (21, 30). pH data collected from the bright Flubi-stained cell body of AtT-20 cells represented both AV-POMC-containing Golgi and some AV-POMC-containing ISGs. MSG pH was measured by collecting data from only the brightly labeled tips of cell processes of AtT-20 cells.

Perfusion and Calibration Solutions and pH Calibration—Ringer's, NH_4Cl Ringer's, and Cl^--free, and sodium-free Ringer's solutions were all prepared as described previously (21). Calibration solutions were also prepared as described previously (21), except the solutions were titrated to the following pH values: 8.2, 7.0, 6.5, 6.0, 5.4, and 4.9. *In situ* calibrations were performed and the data fit to calibration curves, and the calibration curves were used to convert ratio values to pH values exactly as described (21).

Determining H^+ Leak Rates, Buffer Capacities, and H^+ Permeabilities—Rates of H^+ leak out of ER, Golgi, MSG, and plasma membranes were calculated by fitting the data to the single exponential equation: $y = A(1 - e^{-kt})$ using GraphPad InPlot (Kelvin Gee, Irvine, CA). Rate constants (k) and half-times ($t_{1/2}$) were determined from the curve fits.

Since H^+ leak rates across organelle membranes are affected by buffer capacity (β) and surface area-to-volume (S/V) ratio, differences in β or S/V between organelles could account for differences in H^+ leak rates. We accounted for β and S/V ratio values of each organelle by calculating intrinsic H^+ permeabilities, P_{H+}, for ER, Golgi, and MSGs using data from experiments such as those shown in Figs. 3*C* and 4 and the model described below. In order to calculate H^+ permeabilities, we had to first measure β of the cytosol, ER, Golgi, and MSGs of AtT-20 cells. β was calculated from the magnitudes of rapid increases in pH of each compartment during perfusion with solutions containing 20, 30, or 40 mM NH_4Cl or from rapid decreases in pH of compartments during perfusion with solutions containing 20 or 30 mM sodium acetate. Values of β for ER, Golgi, and MSGs were determined using bafilomycin-pretreated cells (500 nM, >2 h) so that the base-line pH values, prior to NH_4Cl or sodium acetate treatment, were similar for all the compartments. For NH_4Cl experiments, using $pK = 9.0$ for the $NH_4^+ \rightarrow H^+ +$

NH_3 reaction and assuming that NH_3 equilibrates equally across all the membranes, β was calculated from the change in pH (extrapolated to time 0) during the switch from Ringer's to NH_4Cl according to (31) Equation 1.

$$\beta = [NH_4^+]/\Delta pH \qquad \text{(Eq. 1)}$$

For sodium acetate experiments, using pK = 4.7 for the $CH_3CO_2H \rightarrow H^+ + CH_3CO_2^-$ reaction and assuming that CH_3CO_2H equilibrates equally across all the membranes, β was calculated from the change in pH (extrapolated to time 0) during the switch from Ringer's to sodium acetate according to Equation 3,

$$\beta = -[CH_3CO_2^-]/\Delta pH \qquad \text{(Eq. 2)}$$

After determining key physical characteristics for each organelle, such as β, a mathematical model for the movement of H^+ across the organelle was required in order to predict the H^+ permeability of the membrane. We employed a model that has been shown to be in quantitative agreement with a diverse range of organelle pH and membrane potential data (26). Our present modeling effort is a subset of this more complete model in that we ignored H^+ pumping by the H^+ v-ATPase, since all the permeability measurements were performed in the presence of bafilomycin. Given this, the measured rate of change of lumenal pH is related to the passive flux of H^+ and the physical characteristics of the organelle as shown in Equation 3,

$$\frac{dpH}{dt} = \frac{1}{\beta_0} \cdot \frac{S}{V} \cdot J_{leak} \qquad \text{(Eq. 3)}$$

where J_{leak} is the total passive flux of H^+ across a unit area of membrane, and β_0 is the organelle buffer capacity. We used surface areas, S, and volumes, V, of ER and Golgi as determined from terminal tubule and acinar cells of the rat submandibular gland (32); S and V of MSGs were based on a 200-m diameter sphere (33). Although our H^+ permeability calculations were determined for AtT-20 (mouse anterior pituitary) cells, we used the S and V values from Taga *et al.* (32) because this was the only published report where S and V for both ER and Golgi membranes were measured in the same cell type.

We modeled the H^+ leak, J_{leak}, as simple passive diffusion. With this assumption, the leak depends on the membrane potential and the concentration gradient as shown in Equation 4,

$$J_{leak} = P_{H^+} \cdot \frac{z \cdot U \cdot ([C_{H^+}]_O - [C_{H^+}]_C \cdot e^{-zU})}{1 - e^{-zU}} \qquad \text{(Eq. 4)}$$

where P_{H+} is the H^+ permeability of the membrane; C_{H+} is the concentration of H^+ in the organelle (O) or cytosol (C); z is the valence of the H^+; and $U = \Psi F/(RT)$, where Ψ is the organelle membrane potential.

We computed Ψ in terms of the excess charge inside the organelle membrane, which was treated as a parallel plate capacitor (Equation 5),

$$\Psi = \frac{F \cdot V}{C_m} \cdot ([K^+]_O - [Cl^-]_O + \int_{pH_O}^{pH_G} \beta_0 \cdot dpH - B) \qquad \text{(Eq. 5)}$$

where C_m is the total capacitance of the membrane (calculated assuming capacitance = 1 microfarad/cm^2); $[K^+]_O$ and $[Cl^-]_O$ are the concentrations of K^+ and Cl^- in the organelle (based on previous experiments, we assumed that K^+ and Cl^- diffuse across organelle membranes according to equations of the form (4)); the integral term represents the total H^+ in the organelle lumen (both buffered and free), and B (a constant) is the concentration of charged species trapped in the organelle. In the absence of any membrane-energizing enzymes, one expects H^+ to diffuse across the organelle membrane until the lumenal pH and the cytosolic pH are equal. However, this is often not the case for organelles that have been treated with bafilomycin (16, 21); furthermore, at rest, the distribution of H^+ across a membrane can be manipulated by the distribution of other ionic species (34). This discrepancy can be attributed to trapped, negatively charged species inside the organelle that, in the absence of an active H^+ v-ATPase, lead to an accumulation of H^+. Our model accounts for the difference in steady-state pH between organelle lumen and cytosol only through changes in the parameter B. Average values of B varied between ~50 and 200 mM. Average B values determined from the model for ER, Golgi, and MSGs did not significantly contribute to the different steady-state pH values of these compartments.

From our buffer capacity measurements, we know that a significant number of H^+ are transported into/out of the organelle during acidification/alkalinization. If this change in charge is not off-set by the subsequent movement of counterions, a large membrane potential will build up across the organelle membrane and quickly limit further changes in pH. This physical insight suggests that organelles that undergo acidification must be permeable to some counterions. However, it is unclear which ions are permeable and how fast their movement is compared with the movement of H^+. Schapiro and Grinstein (25) have convincingly shown that the Golgi is permeable to K^+; they also concluded that the fast dissipation of H^+ gradients in the Golgi by protonophores implied that the counterion movement must be much faster than the endogenous H^+ leak. As discussed under "Results," our present data support these ideas. Therefore, in predicting P_{H+} we assumed that both K^+ and Cl^- were free to diffuse across the organelle membranes. We chose permeability coefficients for these ions of ~10^{-5} cm/s based upon plasma membrane measurements (35). Our numeric results remain unaffected for counterion permeability values down to 10^{-9} cm/s. Below this point, counterion movement becomes the rate-limiting step during alkalinization, which affects predicted P_{H+} values.

Equation 3 and the two additional equations for the passive flux of K^+ and Cl^- combine to form a set of ordinary differential equations (ODE). These ODEs are coupled by the algebraic constraint of Equation 5 and uniquely determine the time course of changes of ionic concentrations in the organelle(s) given an initial set of conditions (*e.g.* initial lumenal concentrations). The model was applied to data recorded using two distinct experimental protocols for inducing organelle alkalinization as follows: (i) as shown in Fig. 4, pH recovery after an NH_4^+ acid-load of cytosol and organelles in the presence of bafilomycin and (ii) as shown in Fig. 3*C*, bafilomycin-induced alkalinization. In both cases, cytosolic K^+ and Cl^- were assumed to remain constant and to be equal to typical cytosolic values ([K^+] = 140 mM; [Cl^-] = 20 mM). Under Cl^--free conditions, cytosolic and organelle [Cl^-] were set to 0. pH_c values were experimentally measured. Before alkalinization began, in both protocols, all compartments reached steady-state pH, indicating that net Cl^- and K^+ fluxes were initially at equilibrium (*i.e.* 0), since Cl^- and K^+ movements were fast. Additionally, the H^+ concentration was initially at equilibrium in the acid-load experiments but not in the bafilomycin-induced alkalinization experiments due to the presence of active H^+ v-ATPases. For a given value of B, the initial lumenal concentrations of ions at equilibrium were uniquely determined from the passive flux equations and Equation 5. With bafilomycin-induced alkalinization, the initial lumenal pH was a free parameter independent of the value of B. In summary, our simulations had two free parameters (P_{H+}, B). The initial organelle pH (pH_o) in the bafilomycin-induced alkalinization experiments was chosen to be the average steady-state pH of the organelle before the addition of bafilomycin. All other parameters were recorded experimentally or determined from equilibrium conditions. As mentioned above, the value B was constrained by the data since it was the only free parameter in the model that accounted for equilibrium differences between pH_c and pH_o.

The free parameters, P_{H+} and B, were determined by using the model to fit the experimentally measured changes of pH_o (Figs. 5 and 6, data points). For every data set, the model ODEs were solved to find which values of P_{H+} and B gave the best fit to the experimental data. Example model fits, from which P_{H+} values were determined, are shown in Figs. 5 and 6 (*solid curves*). The search for the best model fit was performed with a Nelder-Mead algorithm, and the ODEs were solved with a stiff method in both Matlab (Mathworks, Natick, MA) and Berkeley Madonna (George Oster and Robert Macey, University of California, Berkeley).

In experiments in which P_{H+} was calculated from rates of bafilomycin-induced alkalinization (*e.g.* Figs. 3*C* and 6), we assumed pH_c was constant, since bafilomycin had no effect on pH_c (data not shown). In experiments in which P_{H+} was calculated from rates of recovery of pH_o and pH_c following an acid-load, the pH_o recovery was directly dependent upon the recovery of pH_c (see Figs. 4 and 5). To determine P_{H+} using these experimental data, knowledge of the instantaneous H^+ gradient across the organelle membrane was required. Because our experimental system did not permit us to measure pH_c and pH_o in the same cells simultaneously, we undertook the computationally intensive task of fitting all pH_o recovery data against all separately recorded pH_c recovery data. For calculations of P_{H+} in Cl^--free solutions, Golgi and MSG data sets were fit against corresponding measurements of pH_c in Cl^--free solutions. In each of the data runs (*e.g.* 782 runs in the case of the ER data; 17 pH_{ER} data sets × 46 pH_c data sets), a fitness parameter was used in order to determine the likelihood that the pH_o data were a result of a particular pH_c data set. A root mean square fit of the model to the pH_o data was used as a measure of fitness, and its inverse, w, was used as a weight for computing averages and S.E. (Equation 6),

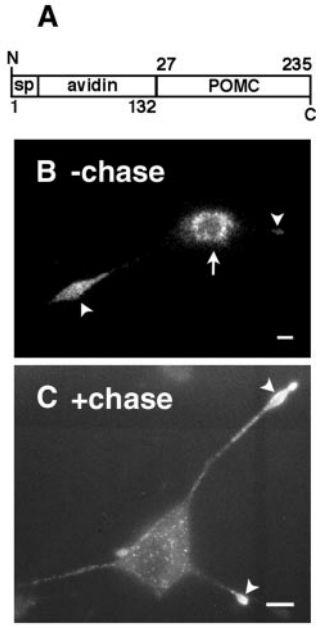

FIG. 1. **Avidin-POMC follows the regulated secretory pathway in AtT-20 cells.** *A,* an AV-POMC chimera protein was constructed by fusing amino acids 1–132 of chicken avidin (signal peptide intact, stop codon removed) with amino acids 27–235 of mouse POMC (signal peptide removed). *sp,* signal peptide. AtT-20 cells expressing AV-POMC were loaded with 3 μM Flubi-2 (4.5 h) and chased for either 1.5 (*B*) or 3 h (*C*) before viewing. After the *longer chase* (*C*), Flubi-2 was chased out of the Golgi (*arrow* in *B*) and into ISGs and MSGs (punctate cell body and tip staining). *Arrow,* cell body staining (Golgi and some ISGs); *arrowheads,* tips of cell processes where MSGs accumulate. *Scale bars*, 10 μm.

$$R = \sqrt{\frac{1}{N}\cdot\sum_{i=1}^{N}(\mathrm{pH}^{i}_{\mathrm{observed}} - \mathrm{pH}^{i}_{\mathrm{mode}})^2} \quad \text{or} \quad w \equiv \frac{1}{R} \qquad \text{(Eq. 6)}$$

where the sum was over all N experimentally measured time points. Chauvenet's criteria were used to exclude three highly improbable predicted permeability values (40). Two sets were rejected because the organelle pH was more alkaline than any cytosolic pH values, and one additional set was rejected due to technical difficulties in finding a reliable best fit.

RESULTS AND DISCUSSION

Targeting Avidin-Chimera Proteins and Flubi Dyes to the ER, Golgi, and MSGs of AtT-20 Cells—ER pH measurements in AtT-20 cells were performed exactly as in HeLa cells (21), where Flubi-2 was loaded into cells expressing avidin-KDEL (AV-KDEL). For AtT-20 Golgi and MSG pH measurements, an avidin-POMC (AV-POMC) chimera protein was expressed, and cells were loaded with Flubi dye to monitor pH. In AtT-20 cells, POMC is a regulated secretory protein that is transported from the ER to the Golgi and packaged into ISGs that mature into MSGs. We constructed an AV-POMC chimera (Fig. 1*A*) that exhibited similar secretion patterns as endogenous POMC in AtT-20 cells (data not shown). Fig. 1*B* shows that live AtT-20 cells loaded with Flubi-2 (4.5 h) and chased briefly (<2 h) showed both cell body staining (Golgi and some ISGs) and staining at the tips of cell processes (MSGs). Longer chase times (>3 h) resulted in the disappearance of Flubi-2 from the Golgi, with increased punctate staining throughout the cell body, particularly concentrated at cell tips, indicating that Flubi-2 had been chased out of the Golgi into MSGs (Fig. 1*C*). Since MSGs are spatially separated from the Golgi, we were able to use AV-POMC-expressing AtT-20 cells to monitor the pH of both proximal (Golgi) and distal (MSGs) compartments of the regulated pathway by restricting data collection to either the cell body or cell tips.

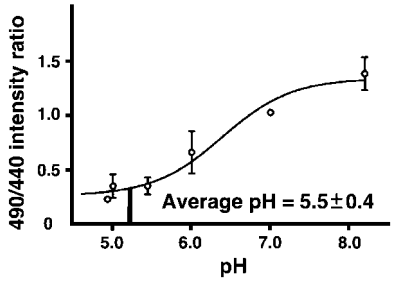

FIG. 2. **Average ratio *versus* pH calibration curve for Flubi-2 in AtT-20 secretory granules.** Calibration solutions containing nigericin and monensin (10 μM each) and titrated to different pH values (8.2, 7.0, 6.0, 5.5, 5.0, and 4.9) were used to generate calibration curves that were used to convert 490 nm/440 nm excitation ratio values (emission = 520–560 nm) to pH values. The *solid line* shows the average $\mathrm{pH}_{\mathrm{MSG}}$ ± S.D. obtained for 24 cells. Average calibration curve *error bars* are from S.E. values.

Flubi-2 for Measuring pH in Secretory Granules, Golgi, and ER of Intact AtT-20 Cells—The pH dependence of the 490/440 nm excitation ratio of Flubi-2 *in situ* within secretory granules of living AtT-20 cells is shown in Fig. 2. Secretory granules were labeled with Flubi-2, and calibration solutions containing nigericin and monensin were perfused onto cells at the end of each experiment. An average calibration curve was generated by plotting 490/440 nm fluorescence ratio *versus* pH of the external solution. $\mathrm{pH}_{\mathrm{MSG}}$ was determined by averaging the steady-state pH of MSGs of cells bathed in pH 7.4 Ringer's solution. $\mathrm{pH}_{\mathrm{MSG}}$ (mean ± S.D.) was 5.5 ± 0.4 (Fig. 2, *solid line*).

We used similar methods to determine ER and Golgi pH values in AtT-20 cells by averaging the steady-state pH values of each compartment of cells bathed in pH 7.4 Ringer's solution. $\mathrm{pH}_{\mathrm{ER}}$ of AtT-20 cells (7.4 ± 0.2) was similar to $\mathrm{pH}_{\mathrm{ER}}$ in HeLa cells (7.2 ± 0.2) (21). In AtT-20 cells, as in HeLa cells, $\mathrm{pH}_{\mathrm{ER}}$ was slightly lower than cytosolic pH (AtT-20 pH_c = 7.6 ± 0.2; HeLa pH_c = 7.4 ± 0.2). In AtT-20 cells, pH_{G} was 6.2 ± 0.4, similar to values measured for the Golgi in non-regulated cells (15, 16, 21). Thus, the pH of the Golgi compartments in live, intact endocrine cells appears acidic and similar to the Golgi pH in non-regulated cells. Although the Flubi-2 staining in the cell body (Fig. 1*B*) may consist of signals from both Golgi and ISGs, the majority of these signals come from the Golgi compartments and not the ISGs. This latter conclusion is based on the observation that brefeldin A, which causes Golgi but not trans-Golgi network and post-Golgi organelles to redistribute to the ER (36), causes complete dispersal of the perinuclear POMC staining to the ER (data not shown). Future experiments using avidin constructs targeted specifically to individual cisternae of the Golgi complex and the ISGs will be necessary to resolve the likely small pH differences between these compartments.

Are Cl^- or K^+ Conductances Determinants of Steady-state pH_{MSG} or the H^+ Leak Out of MSGs?—Early models of pH regulation in secretory granules suggested that the assumed inside positive organelle membrane potential limited H^+ accumulation by the H^+ v-ATPase and that a Cl^- conductance was required to shunt this potential to allow adequate acidification of organelles (9). We examined the potential role of Cl^- conductance in regulating $\mathrm{pH}_{\mathrm{MSG}}$ in AtT-20 cells by replacing all Cl^- with gluconate in the extracellular solution of intact Flubi-2-loaded, AV-POMC-expressing AtT-20 cells. We assumed that cytosolic Cl^- would be depleted after a long (>20 min) incubation in Cl^--free solution, since for plasma membrane Cl^- permeabilities between 10^{-5} and 10^{-6} cm/s (35), the half-time for cytosolic Cl^- depletion from a 1000-μm^3 cell is 100–200 s. This calculation follows from Equation 4 (see "Experimental Procedures") but neglects the inside negative membrane potential

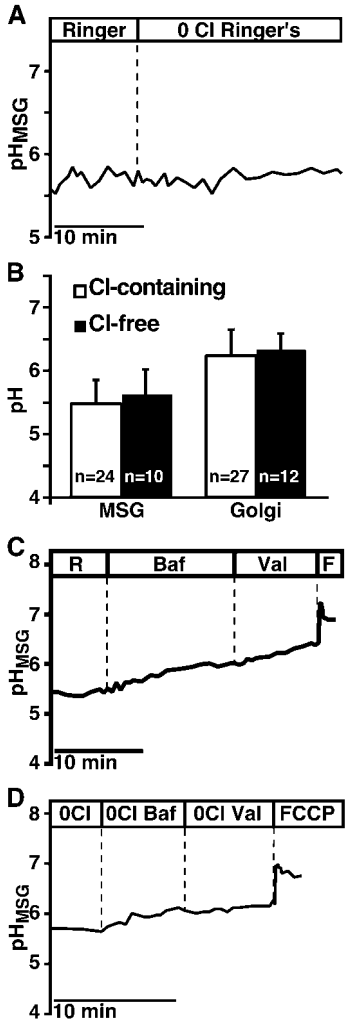

FIG. 3. **AtT-20 MSG steady-state pH and the H^+ leak out are not regulated by Cl^- or K^+ counterion conductances.** Removal of Cl^- (*0 Cl Ringer's*, replaced with gluconate) from the extracellular solution had no effect on pH_G or pH_{MSG} in intact cells, as shown by a typical experiment (*A*) and by quantitating the results from numerous experiments (*B*). *C,* treatment with bafilomycin (*Baf*) (H^+ v-ATPase inhibitor, 500 nM) caused pH_{MSG} to alkalinize. Addition of the K^+ ionophore, valinomycin (*Val*) (10 μM), did not affect the rate of alkalinization; however, FCCP (*F*) (protonophore, 20 μM) caused rapid alkalinization of pH_{MSG}. *F*, FCCP; *R*, Ringer's. Similar experiments in Cl^--free solutions gave similar results (*D*). The experiments shown in *C* and *D* were repeated three times with the same results.

that is likely to exist in AtT-20 cells. In all likelihood, the membrane potential and also the presence of neutral transporters (*e.g.* NaKCl cotransport) will cause the half-time for Cl^- depletion to be shorter than 100–200 s, ensuring that cell [Cl] will probably be lower than 1 mM after about 10 min. We expected that if Cl^- were required to provide a counterion for the accumulation of lumenal H^+, then incubation in Cl^--free solution for 30 min would reduce the acidity of MSGs. Similar to previous experiments on the Golgi of Chinese hamster ovary and HeLa cells (18, 21, 25), treatment with Cl^--free solution did not affect steady-state pH_{MSG} over the course of >30 min (Fig. 3*A*), indicating that Cl^- was not required to maintain acidic MSGs. A summary of results from experiments such as the one in Fig. 3*A* is shown in Fig. 3*B*. In Cl^--containing solutions pH_{MSG} (mean ± S.D.) was 5.5 ± 0.4, nearly the same as pH_{MSG} in Cl^--free solutions, 5.6 ± 0.4; pH_G was 6.3 ± 0.3 in Cl^--free solutions, insignificantly different from pH_G obtained in Cl^--containing solutions, 6.2 ± 0.4.

We also tested for the role of K^+ and Cl^- conductances in determining the acidity in MSGs and Golgi using a different approach. As shown in Fig. 3*C*, cells were treated first with 500 nM bafilomycin (H^+ v-ATPase inhibitor) which caused pH_{MSG} to alkalinize. This result showed that pH_{MSG} was maintained by constantly active, bafilomycin-sensitive, H^+ v-ATPases opposing H^+ leaks. The rate of H^+ leak out of the acidic MSGs into the pH 7.4 cytosol is a function of the H^+ permeability, transmembrane pH gradient, and membrane potential (which, in the presence of bafilomycin, is a function of the conductances to the major ionic constituents of the cytosol, K^+, and Cl^-). If the K^+ conductance were limiting the rate of H^+ leak through effects on membrane potential, then addition of valinomycin (K^+ ionophore) should increase both the K^+ conductance and also the rate of H^+ leak out of MSGs. As shown in Fig. 3*C*, addition of 10 μM valinomycin did not affect the rate of bafilomycin-induced MSG alkalinization; the rate of alkalinization increased only upon treatment with the protonophore FCCP (20 μM). This result indicated that in the presence of valinomycin, the H^+ conductance was limiting the rate of H^+ leak out of the MSGs. Similar experiments were performed on cells bathed in Cl^--free solutions for >30 min to reduce cell [Cl^-] (Fig. 3*D*). By incubating the cells in Cl^--free solution, we expected that the major counterion conductance (for H^+) across MSG membranes would now be due solely to K^+. If the K^+ conductance were smaller than the H^+ conductance, then during bafilomycin treatment H^+ would leak out of the MSGs only as fast as K^+ leaked into the MSGs, and the rate of alkalinization would be increased by valinomycin. However, valinomycin had no effect on the rate of H^+ leak out of MSGs in the absence of Cl^- (Fig. 3*D*). Again, the H^+ leak out of the MSGs increased only when the cells were treated with FCCP.

The simplest conclusion from these experiments was that the conductances to both Cl^- and K^+ were larger than the H^+ conductance for both MSGs and Golgi. Because the conductance to K^+ was large, removing Cl^- (eliminating Cl^- as a counterion) had no effect on either the ability of MSGs to acidify their lumens in control cells or on the rates of passive H^+ flux out of the lumen in bafilomycin-treated cells. The K^+ conductance appeared to be larger than the H^+ conductance because valinomycin did not affect H^+ flux in Cl^--free solutions (when the rate of H^+ exit from the MSGs is determined by the H^+ permeability and the rate of K^+ entry). Thus, it appeared that the Golgi compartments in both regulated AtT-20 cells and non-regulated HeLa cells (21, 25) had similar pH values and were also highly conductive to both K^+ and Cl^-.

Our conclusion that MSGs did not require Cl^- to generate normal lumenal acidity contradicts previous conclusions (9, 22). However, it should be noted that these previous experiments were non-quantitative pH measurements using acridine orange in isolated synaptic vesicles *in vitro*; furthermore, the dose-dependent requirement for Cl^- in acidification of the secretory vesicles was accomplished by changing the concentrations of *both* K^+ *and* Cl^-, and the role of Cl^- alone or K^+ alone was not determined. The contradictory Cl^- results may also have been due to different pH regulatory mechanisms present in organelles of the endocytic pathway *versus* organelles of the secretory pathway. Early studies of pH regulation in the endocytic pathway indicated that endosome acidification could be regulated by altering the membrane potential by changing the Cl^- conductance or the Na/K-ATPase activity (37, 38). Perhaps the conflicting Cl^- data reflect two sets of organelles with distinct pH regulatory mechanisms as follows: (i) organelles of the endocytic recycling pathway (including synaptic vesicles), where membrane potential and thus Cl^- are important regulators of pH, and (ii) organelles of the biosynthetic secretory pathway (ER, Golgi, secretory granules), where organelle pH is

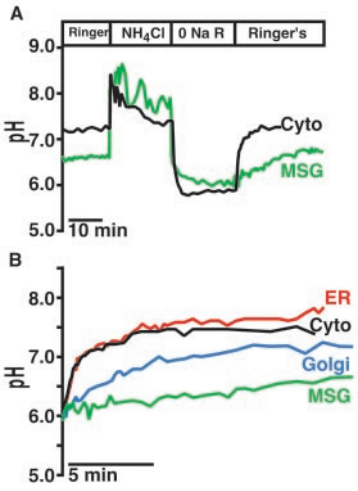

FIG. 4. **pH recoveries of AtT-20 cell compartments after an acid load.** The pH recoveries of cytosol, ER, Golgi, and MSGs were measured in either BCECF-AM-loaded or Flubi-2-loaded, bafilomycin-pretreated, intact cells by acid-loading the cytosol (*Cyto*) and organelles with an NH_3/NH_4^+ pulse, followed by a washout with sodium-free Ringer's (*0 Na R*) before allowing the pH values to recover in sodium-containing Ringer's (*Ringer's*). This protocol is illustrated in *A* with typical results for cytosol (*black*) and MSG (*green*) pH. *B,* only the pH recovery traces for each organelle are shown.

not regulated by Cl^- or K^+ conductances.

Measuring H^+ Leak Rates and Intrinsic H^+ Permeabilities across ER, Golgi, and MSG Membranes in AtT-20 Cells—The data presented above were consistent with the hypothesis that the MSG membrane was likely to have large conductances to both K^+ and Cl^- but lower conductance/permeability to H^+. Under these conditions, pH_{MSG} was limited by the magnitude of the H^+ "leak" or "permeability" pathway. Based on our previous work on ER and Golgi pH regulation in HeLa cells (21) and the finite H^+ permeability of phospholipid bilayers (10^{-4} cm/s, (39)), we hypothesized that the pH differences between the ER, Golgi, and secretory granules in AtT-20 cells might be generated by gradually decreasing the H^+ leak or permeability along the secretory pathway. To gain insights into H^+ leak rates across AtT-20 ER, Golgi, and MSG membranes, we followed the same acid-loading protocol we used to measure rates of pH recoveries for organelles of HeLa cells (21). AtT-20 pH_c measurements were performed on cells loaded with the well known cytosolic pH dye, BCECF-AM (2 μM loaded 1 h, 1-h chase). AtT-20 cells expressing either AV-KDEL or AV-POMC were loaded with Flubi-2 (at least 4 h), chased (0–2 h), and treated with 500 nM bafilomycin (at least 2 h) before measuring pH_c, pH_{ER}, pH_G, and pH_{MSG}. AtT-20 cells were acid-loaded by incubating in 40 mM NH_4Cl for 20 min. When the NH_4Cl solution was replaced with sodium-free Ringer's, pH_c, pH_{ER}, pH_G, and pH_{MSG} remained acidic until sodium-containing Ringer's was returned to the chamber, at which point pH_c recovered rapidly to pH 7.4, and the ER, Golgi, and MSGs leaked out H^+ to recover their pH values. This protocol is illustrated in Fig. 4*A*, which shows typical pH traces for cytosol (*black*) and MSG (*green*) compartments. Fig. 4*B* shows the representative pH recoveries for each compartment, cytosol (*black*), ER (*red*), Golgi (*blue*), and MSGs (*green*), as the outside solution was switched from sodium-free to sodium-containing Ringer's.

The data for the pH recoveries of AtT-20 cytosol, ER, Golgi, and MSGs were fit to single exponential equations to obtain half-times ($t_{1/2}$) for the pH recovery of each compartment. The results from these calculations have been summarized in Table I. ER membranes had the fastest pH recovery ($t_{1/2}$ = 59 s),

TABLE I
Half-times for pH recoveries of the cytosol, ER, Golgi, and MSGs of AtT-20 cells

The data for the pH recoveries of the cytosol, ER, Golgi, and MSG from experiments such as those shown in Fig. 4*B* were fit to the single exponential equation: $y = A(1 - e^{-kt})$. From each curve fit, a rate constant (k) and $t_{1/2}$ value, representing the half-time for the pH recovery of the cytosol or organelle, were obtained. The $t_{1/2}$ *values are presented as mean ± S.E.*

AtT-20 compartment	$t_{1/2}$	*n*
	(s)	
Cytosol	40 ± 2	30
ER	59 ± 5	17
Golgi	283 ± 87	11
MSG	734 ± 184	10

indicating a large ER H^+ leak that quickly equilibrated pH_{ER} and pH_c (cytosol $t_{1/2}$ = 40 s). This result is very similar to results obtained on HeLa cells (21). In AtT-20 cells, just as in HeLa cells, more distal organelles had slower pH recoveries compared with ER and cytosol. The pH recovery out of the Golgi ($t_{1/2}$ = 283 s) was almost 5 times slower than the ER; the pH recovery of MSGs ($t_{1/2}$ = 734 s) was 2.5 times slower than that of the Golgi and 12 times slower than that of the ER.

These data suggested that organelles in the regulated secretory pathway exhibited decreasing H^+ leak rates, which may be a major contributor to the decreasing steady-state pH values of these organelles. However, the decreasing H^+ leak rates we measured could also have been the result of increasing buffer capacities of organelles along the secretory pathway, or these results could have been due to differences in the surface area-to-volume (*S/V*) ratios of secretory pathway organelles. Therefore, to account for buffer capacities and *S/V* ratios, we determined the intrinsic H^+ permeability, P_{H+}, for each organelle membrane (ER, Golgi, and MSG).

Buffer capacities (mean ± S.E. mM/pH) were determined (as described under "Experimental Procedures") for the cytosol (23 ± 3, n = 38), ER (17 ± 3, n = 21), Golgi (26 ± 6, n = 10), and MSG (20 ± 6, n = 10) compartments. By using these mean buffer capacity values and previously estimated surface areas and volumes (32, 33), the data from acid-load recovery experiments (Fig. 4*B*) were fit (Fig. 5) using the mathematical organelle pH model (described under "Experimental Procedures") to determine P_{H+} for the ER, Golgi, and MSG membranes. Fig. 5 shows typical organelle pH recovery data (*colored data points*), the corresponding best pH_c recovery (*black*), and the model curve fits (*colored solid curves*, determined using Equations 3–5). P_{H+} values are listed in Table II, which shows that P_{H+} decreased progressively from the ER (P_{H+} = 51 × 10^{-4} cm/s) to Golgi (P_{H+} = 21 × 10^{-4} cm/s) to MSGs (P_{H+} = 3 × 10^{-4} cm/s). The P_{H+} that we estimated for ER (51 × 10^{-4} cm/s) should be considered a lower estimate since these measurements may have been limited by the rates of pH_c recovery, which were controlled by plasma membrane pH regulatory mechanisms. The P_{H+} value for each organelle was statistically different ($p < 0.07$) from the other organelles.

In addition to using pH recovery data from acid-loaded cells and organelles, we also estimated P_{H+} for Golgi and MSG membranes using H^+ leak data obtained from bafilomycin-treated cells. By using H^+ leak data from experiments such as the one shown in Fig. 3*C,* we fit the bafilomycin-induced alkalinization rate using the mathematical organelle pH model as shown in Fig. 6. The main difference between the bafilomycin-induced alkalinization experiments and the acid-load pH recovery experiments was that using the former protocol pH_c remained constant (data not shown) since bafilomycin had no effect on pH_c, whereas using the latter protocol pH_c acidified and changed as pH_o changed (*e.g.* Fig. 4). For both protocols,

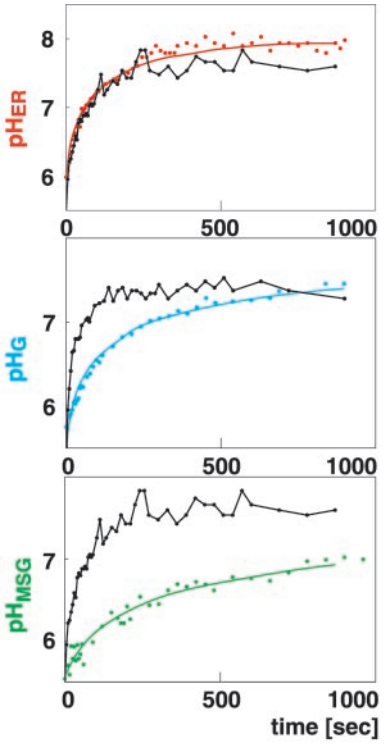

FIG. 5. **Fitting pH recovery data to a mathematical pH model to determine H^+ permeability.** Representative model fits (*red, blue,* and *green curves*) of ER, Golgi, and MSG acid-load pH recovery data (*red, blue,* and *green data points*) are shown with their corresponding cytosolic runs (*black*) that gave rise to these fits. For the model fits shown, P_{H+}(ER) = 44.3× 10^{-4} cm/s, P_{H+}(G) = 12 × 10^{-4} cm/s, and P_{H+}(MSG) = 2.8 × 10^{-4} cm/s. Values of P_{H+} were determined from the best model fit to the experimental data and are summarized in Table II.

TABLE II

H^+-permeabilities determined from rates of pH recoveries of the ER, Golgi, and MSGs of AtT-20 cells

Data from pH recoveries (Figs. 4*B* and 5), measured buffer capacities (β), and previously determined surface area-to-volume ratios (32, 33) were incorporated to determine the intrinsic H^+ permeabilities (P_H) of AtT-20 ER, Golgi, and MSG membranes using the Berkeley Madonna (G. Oster and R. Macey, University of California, Berkeley) modeling program. β and P_H values are presented as mean ± S.E. P_H values for each organelle were compared using the Welch test: ER *versus* Golgi ($p < 0.07$), Golgi *versus* MSG ($p < 0.07$), and ER *versus* MSG ($p < 0.02$).

AtT-20 membrane	β	Surface (μm^2)/ volume (μm^3)	P_H^+ (× 10^{-4} cm/s)
	mM/pH		
ER (n = 16)	17 ± 3	1110/35.4	51 ± 11
Golgi (n = 10)	26 ± 6	514/26.4	21 ± 9
MSG (n = 10)	20 ± 6	0.126/0.00419	3 ± 1

TABLE III

H^+ permeabilities determined from rates of bafilomycin-induced alkalinization of the ER, Golgi, and MSGs of AtT-20 cells

Data from bafilomycin-induced alkalinization rates measured in Cl^--containing (*e.g.* Fig. 3*C*) and Cl^--free (*e.g.* Fig. 3*D*) solutions, together with measured buffer capacities and previously determined surface area-to-volume ratios (see Table II), were incorporated to determine the intrinsic H^+ permeabilities (P_{H^+}) of AtT-20 Golgi and MSG membranes using the Berkeley Madonna modeling program. P_{H^+} values are presented as mean ± S.E. Golgi P_{H^+} values determined in the presence and absence of Cl^- were statistically the same according to the Student's t test. MSG P_{H^+} values determined in the presence and absence of Cl^- were also statistically the same according to the Student's t test.

AtT-20 membrane	P_H	Cl^--free P_{H^+}
	(× 10^{-4} *cm/s*)	
Golgi	1.3 ± 0.4 (n = 5)	1.6 ± 0.6 (n = 6)
MSG	0.35 ± 0.1 (n = 9)	0.6 ± 0.35 (n = 7)

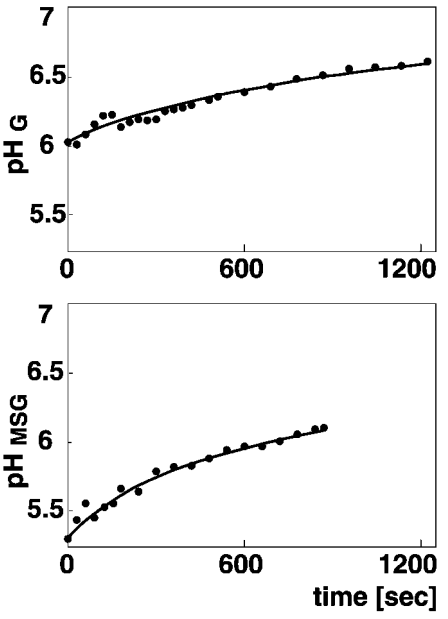

FIG. 6. **Fitting bafilomycin-induced alkalinization data to a mathematical pH model to determine H^+ permeability.** Representative model fits (*curves*) of Golgi and MSG bafilomycin-induced H^+ leak data (*data points*) are shown. Bafilomycin had no effect on pH_c; thus we assumed a constant pH_c (7.58 ± 0.19, n = 187 cells) for the model fits. For the model fits shown, P_{H+}(G) = 1.6 × 10^{-4} cm/s, P_{H+}(MSG) = 0.3 × 10^{-4} cm/s. Values of P_{H+} were determined from the best model fit to the experimental data and are summarized in Table III.

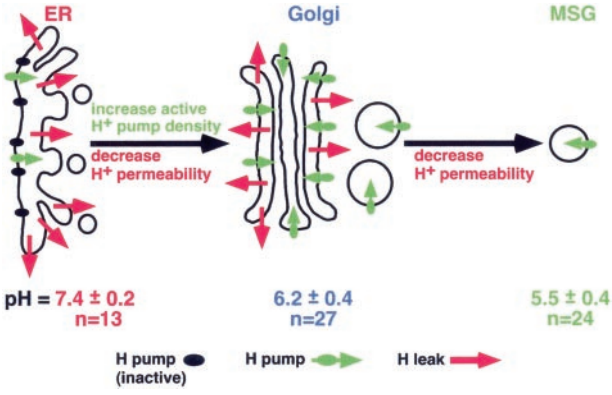

FIG. 7. **A model for pH regulation in the regulated secretory pathway.** pH_{ER} (mean ± S.D.) in AtT-20 cells was 7.4 ± 0.2 (n = 13); pH_G was 6.2 ± 0.4 (n = 27), and pH_{MSG} was 5.5 ± 0.4 (n = 24). pH_G and pH_{MSG} were maintained by constantly active, bafilomycin-sensitive, H^+ v-ATPases that opposed H^+ leaks. MSG membranes had large conductances to both Cl^- and K^+ compared with H^+. Our data indicate that, to generate the stepwise acidification from ER to Golgi to MSGs, the density of active H^+ pumps must progressively increase, while the H^+ permeability gradually decreases.

the pH gradient between the cytosol and organelle lumen was taken into account in the modeling (see Equation 4 under "Experimental Procedures"). By using the bafilomycin-induced alkalinization protocol, we calculated P_{H+} values of Golgi and MSG membranes to be lower than those calculated using acid-load pH recovery data, but the P_{H+} for MSGs was consistently lower than the P_{H+} of Golgi membranes. These data are summarized in the first two columns of Table III.

The data from Fig. 3 indicated that Cl^- was not required to maintain an acidic steady-state pH_{MSG}. We further tested for the potential role of Cl^- conductance in controlling Golgi and MSG membrane potential by determining the H^+ permeability in Cl^--free solutions. In the presence of bafilomycin, the H^+ leak across MSG membranes will be a function of membrane

potential and pH gradient, and if Cl^- conductance were important for shunting membrane potential, then we would expect that the calculated P_{H+} would be smaller for experiments in Cl^--free *versus* Cl^--containing solutions. To determine whether P_{H+} of MSGs was Cl^--dependent, we used data from Cl^--free bafilomycin-induced alkalinization experiments (*e.g.* Fig. 3*D* and Fig. 6) to determine the P_{H+} of MSG membranes in the absence of Cl^- (Table III). The P_{H+} in Cl^--free solutions was 1.6×10^{-4} cm/s for Golgi membranes and 0.6×10^{-4} cm/s for MSG membranes, in both cases greater than the H^+ permeabilities measured in Cl^--containing solutions (Golgi = 1.3×10^{-4} cm/s MSG = 0.35×10^{-4} cm/s), indicating that Cl^- was not required for the H^+ leak out of either the Golgi or MSGs in AtT-20 cells.

Summary, a Model for pH Regulation in the Regulated Secretory Pathway—This study constitutes the first investigation into the dynamics of pH regulation in organelles of the secretory pathway of live, intact endocrine cells, where the organelle acidification process is crucial for the sorting and processing of regulated secretory hormones. We determined that, just as for the ER and Golgi of HeLa cells, the steady-state pH values of AtT-20 ER, Golgi, and MSGs appeared to be controlled primarily by rates of H^+ v-ATPase pumping and by the magnitude of H^+ leaks. Our data and mathematical modeling showed that the membrane potential in Golgi and MSGs of AtT-20 cells was small and not perturbed by large changes in Cl^- and K^+ conductances; these results indicated that membrane potential was not a determinant of steady-state Golgi and MSG pH values.

We previously found in HeLa cells that the rate of H^+ leak out of the Golgi was three times slower than the H^+ leak out of the ER (21). In AtT-20 cells, the rates of H^+ leak steadily decreased from ER to Golgi to MSGs, with MSGs having a 12 times slower leak rate than ER membranes. After accounting for buffer capacities and *S/V* ratios, and with the realization that the calculated P_{H+} of the ER was likely to be somewhat underestimated (see above), we conclude that P_{H+} of the ER was twice as large as that of the Golgi which was 4–7 times greater than MSGs. The variability of our calculated P_{H+} values stemmed in part from the variability in the experimentally determined buffer capacity (β) values. The experimental determination of β is prone to large variabilities due to different rates of mixing of NH_3/NH_4^+ solutions into the chamber, possible contributions of pH regulatory mechanisms in the organelle and plasma membranes, and the finite permeability of membranes to NH_4^+. We tried to limit these factors as much as possible by performing experiments in sodium-free solutions following bafilomycin treatment, but it is nearly impossible to eliminate these complicating factors completely. Furthermore, the buffer capacity experiments were performed separately from the experiments used to determine P_{H+}. It is likely that our error bars for P_{H+} would have been smaller had we been able to perform the buffer capacity experiments and H^+ leak experiments in the same cells and then use the β value for a particular cell to calculate the P_{H+} for that cell.

Are the differences in H^+ permeabilities sufficient to account for the different steady-state pH values of the ER, Golgi, and MSGs? Alternatively, are concomitant increases in H^+ pumping activity required to establish the stepwise decreases in pH between these organelles? To answer these questions, we used the previously published organelle pH model (26) that describes both H^+ pumping and H^+ leaking. By using this model, along with our experimentally determined Golgi and MSG buffer capacities and estimated Golgi and MSG P_{H+} and *S/V* values (32, 33), we found that generating the >1.0 unit pH drop from the ER (pH 7.4) to Golgi (pH 6.2) required either a 10-fold increase in the active H^+ pump density (assuming the H^+ pump activity of each H^+ v-ATPase is constant) or a 10-fold decrease in P_{H+} between the ER and Golgi. Generating the 0.7 unit pH drop between Golgi (pH 6.2) and MSGs (pH 5.5) required either a 5-fold increase in active H^+ pump density or a 5-fold decrease in P_{H+} between Golgi and MSGs.

Since our calculated P_{H+} values (Table II) for the ER and Golgi differed by 2-fold rather than 10-fold, an increase in H^+ pump activity must have accompanied the 2-fold decrease in P_{H+} to generate the lower pH of the Golgi compared with the ER. These calculations, together with previous data showing that bafilomycin treatment had no effect on steady-state pH_{ER} of Vero and HeLa cells (17, 21), indicate that for AtT-20 cells, the Golgi had a higher density of active H^+ v-ATPases compared with the ER. Based on the acid-load pH recovery data (Table II), our estimated P_{H+} values for Golgi and MSGs differed by 7-fold. When we used the rate of alkalinization due to bafilomycin treatment (Table III) to calculate P_{H+}, P_{H+} for Golgi and MSGs differed by only 4-fold. It is unclear why the different protocols (pH recovery after an acid-load *versus* bafilomycin-induced alkalinization) for measuring the H^+ leak out of organelles produced different H^+ permeability values for Golgi and MSGs. The main difference between the two protocols was the effect on pH_c. In the bafilomycin-induced H^+ leak protocol, pH_c was ~7.4 and remained constant throughout the protocol. In the NH_3/NH_4^+ acid-load protocol, pH_c acidified to <6.5 and then alkalinized throughout most of the protocol. In the acid-load protocol, pH_o recovery was directly dependent upon the recovery of pH_c. The different P_{H+} values measured using the different protocols could be explained by a pH-dependent H^+ leak across the organelle membrane which would increase as pH_c decreased. In the acid-load protocol, the acidic initial pH_c would result in a much faster P_{H+} than in the bafilomycin protocol, where pH_c is neutral. Since both protocols had their advantages and disadvantages, we chose to present the data obtained by both protocols rather than select one data set over the other. Most likely, the difference in P_{H+} between Golgi and MSGs in AtT-20 cells lies somewhere between 7- and 4-fold. Both data sets are consistent with a gradual decrease in organelle H^+ permeability from ER to Golgi to secretory granules. Our working model for organelle pH regulation along the regulated secretory pathway is illustrated in Fig. 7. Based on our experimental and modeling results, we conclude that the decreasing pH values of organelles of the regulated secretory pathway is established by gradually increasing the density of active H^+ pumps from ER to Golgi while concomitantly decreasing the H^+ permeability from ER to Golgi to MSGs.

Acknowledgments—We thank J. Llopis (University of California, San Diego, currently at the Universidad de Castilla, La Mancha) for the AV-KDEL plasmid, M. Kulomaa (University of Jyvaskyla, Finland) for the avidin clone, and K. Teter for the AV-POMC construct and the AtT-20 AV-POMC stable cell line. We thank Juan Llopis and members of the Machen and Moore labs for helpful discussions.

REFERENCES

1. Schmidt, W. K., and Moore, H. P. (1995) *Mol. Biol. Cell* **6,** 1271–1285
2. Gerdes, H. H., Rosa, P., Phillips, E., Baeuerle, P. A., Frank, R., Argos, P., and Huttner, W. B. (1989) *J. Biol. Chem.* **264,** 12009–12015
3. Chanat, E., and Huttner, W. B. (1991) *J. Cell Biol.* **115,** 1505–1519
4. Colomer, V., Kicska, G. A., and Rindler, M. J. (1996) *J. Biol. Chem.* **271,** 48–55
5. Arvan, P., and Castle, D. (1998) *Biochem. J.* **332,** 593–610
6. Hutton, J. C. (1982) *Biochem. J.* **204,** 171–178
7. Orci, L., Ravazzola, M., Amherdt, M., Madsen, O., Perrelet, A., Vassalli, J. D., and Anderson, R. G. (1986) *J. Cell Biol.* **103,** 2273–2281
8. Orci, L., Ravazzola, M., Storch, M. J., Anderson, R. G., Vassalli, J. D., and Perrelet, A. (1987) *Cell* **49,** 865–868
9. Barasch, J., Gershon, M. D., Nunez, E. A., Tamir, H., and al-Awqati, Q. (1988) *J. Cell Biol.* **107,** 2137–2147
10. Orci, L., Halban, P., Perrelet, A., Amherdt, M., Ravazzola, M., and Anderson, R. G. (1994) *J. Cell Biol.* **126,** 1149–1156
11. Urbe, S., Dittie, A. S., and Tooze, S. A. (1997) *Biochem. J.* **321,** 65–74
12. Miesenböck, G., De Angelis, D. A., and Rothman, J. E. (1998) *Nature* **394,**

192–195
13. Anderson, R. G. W., and Pathak, R. K. (1985) *Cell* **40,** 635–643
14. Schwartz, A. L., Strous, G. J., Slot, J. W., and Geuze, H. J. (1985) *EMBO J.* **4,** 899–904
15. Seksek, O., Biwersi, J., and Verkman, A. S. (1995) *J. Biol. Chem.* **270,** 4967–4970
16. Kim, J. H., Lingwood, C. A., Williams, D. B., Furuya, W., Manolson, M. F., and Grinstein, S. (1996) *J. Cell Biol.* **134,** 1387–1399
17. Kim, J. H., Johannes, L., Goud, B., Antony, C., Lingwood, C. A., Daneman, R., and Grinstein, S. (1998) *Proc. Natl. Acad. Sci. U. S. A.* **95,** 2997–3002
18. Demaurex, N., Furuya, W., D'Souza, S., Bonifacino, J. S., and Grinstein, S. (1998) *J. Biol. Chem.* **273,** 2044–2051
19. Llopis, J., McCaffery, J. M., Miyawaki, A., Farquhar, M. G., and Tsien, R. Y. (1998) *Proc. Natl. Acad. Sci. U. S. A.* **95,** 6803–6808
20. Farinas, J., and Verkman, A. S. (1999) *J. Biol. Chem.* **274,** 7603–7606
21. Wu, M. M., Llopis, J., Adams, S., McCaffery, J. M., Kulomaa, M. S., Machen, T. E., Moore, H. P., and Tsien, R. Y. (2000) *Chemistry and Biology* **7,** 197–209
22. Maycox, P. R., Deckwerth, T., Hell, J. W., and Jahn, R. (1988) *J. Biol. Chem.* **263,** 15423–15428
23. Stobrawa, S. M., Breiderhoff, T., Takamori, S., Engel, D., Schweizer, M., Zdebik, A. A., Bosl, M. R., Ruether, K., Jahn, H., Draguhn, A., Jahn, R., and Jentsch, T. J. (2001) *Neuron* **29,** 185–196
24. Al-Awqati, Q. (1986) *Annu. Rev. Cell Biol.* **2,** 179–199
25. Schapiro, F. B., and Grinstein, S. (2000) *J. Biol. Chem.* **275,** 21025–21032
26. Grabe, M., and Oster, G. (2001) *J. Gen. Physiol.* **117,** 329–343
27. Chavez, R. A., Chen, Y. T., Schmidt, W. K., Carnell, L., and Moore, H. P. (1994) *Methods Cell Biol.* **43,** 263–288
28. Grote, E., Hao, J. C., Bennett, M. K., and Kelly, R. B. (1995) *Cell* **81,** 581–589
29. McNeil, P. L., Murphy, R. F., Lanni, F., and Taylor, D. L. (1984) *J. Cell Biol.* **98,** 1556–1564
30. Teter, K., Chandy, G., Quiñones, B., Pereyra, K., Machen, T., and Moore, H. P. (1998) *J. Biol. Chem.* **273,** 19625–19633
31. Roos, A., and Boron, W. F. (1981) *Physiol. Rev.* **61,** 296–434
32. Taga, R., Alvares, E. P., and Sesso, A. (1993) *Arch. Histol. Cytol.* **56,** 517–523
33. Gumbiner, B., and Kelly, R. B. (1981) *Proc. Natl. Acad. Sci. U. S. A.* **78,** 318–322
34. Langridge-Smith, J. E., and Dubinsky, W. P. (1986) *J. Membr. Biol.* **94,** 197–204
35. Hartmann, T., and Verkman, A. S. (1990) *Biophys. J.* **58,** 391–401
36. Chege, N. W., and Pfeffer, S. R. (1990) *J. Cell Biol.* **111,** 893–899
37. Cain, C. C., Sipe, D. M., and Murphy, R. F. (1989) *Proc. Natl. Acad. Sci. U. S. A.* **86,** 544–548
38. Fuchs, R., Schmid, S., and Mellman, I. (1989) *Proc. Natl. Acad. Sci. U. S. A.* **86,** 539–543
39. Paula, S., Volkov, A. G., Van Hoek, A. N., Haines, T. H., and Deamer, D. W. (1996) *Biophys. J.* **70,** 339–348
40. Taylor, J. R. (1982) *An Introduction to Error Analysis* (Commins, E. D., ed) pp. 141–152, University Science Books, Mill Valley, CA